16TH EUROPEAN CONFERENCE ON EARTHQUAKE ENGINEERING THESSALONIKI 18 - 21 JUNE 2018

DESIGN, NUMERICAL SIMULATION, AND EXPERIMENTAL EVALUATION OF A ROCKING DAMAGE-FREE STEEL COLUMN BASE WITH FRICTION DEVICES

Fabio FREDDI[1], Christoforos A. DIMOPOULOS[2], Theodore L. KARAVASILIS[3]

ABSTRACT

Conventional seismic-resistant structures, such as steel moment resisting frames, are designed to experience significant inelastic deformations under strong earthquakes. Inelastic deformations result in damage in structural members and residual interstory drifts, which lead to high repair costs and disruption of the building use or occupation. The aforementioned socio-economic risks highlight the need for widespread implementation of minimal-damage structures, which can reduce both repair costs and downtime. Examples of such structures include steel frames equipped with post-tensioned beam-column connections, passive energy dissipation devices, self-centering braces, and other smart structural details. These earthquake-resilient steel frame typologies have been extensively studied during the last decade but little attention has been paid to the behaviour of their column bases. The paper presents an experimental program on a damage-free rocking steel column base which uses post-tensioned high-strength steel bars to control rocking behaviour and friction devices to dissipate seismic energy. Contrary to conventional steel column bases, the proposed rocking column base exhibits monotonic and cyclic moment–rotation behaviours that are easily described using simple analytical equations. The latter allow the development of a practical step-by-step design procedure, which ensures damage-free behaviour, self-centering capability, and adequate energy dissipation capacity for a predefined target column base rotation. The experimental behaviour of the column base under monotonic and cyclic loading protocols confirm its self-centering and damage-free behaviour even under very large rotations.

Keywords: Column base; Steel frames; Seismic design; Experimental Assessment; Resilience.

1. INTRODUCTION

Earthquake-resilient steel frame typologies have been extensively studied during the last decade (Christopoulos and Filiatrault 2006, Chancellor *et al.* 2014) but little attention has been paid to their column bases. Conventional steel column bases consist of an exposed steel base plate secured to the concrete foundation using steel anchor rods typically designed as full-strength so that plastic hinges are developed in the bottom end of the first story columns (Eurocode 3, Eurocode 8). Plastic hinges in the columns induce non-repairable damage. Moreover, this design approach needs very strong column bases with adequate over-strength to account for material variability (Latour and Rizzano 2013a). Eurocode 8 allows also the design of partial-strength column bases, which are designed to develop plastic deformations, however, such design philosophy needs the knowledge of the plastic rotation capacity of the column base under cyclic loading, which is difficult to predict (Latour and Rizzano 2013b, Kanvinde *et al.* 2012). Most importantly, field observations after strong earthquakes confirmed the susceptibility of column bases to difficult-to-repair damage such as concrete crushing, weld fracture, anchor rod fracture, and base plate yielding (Grauvilardell *et al.* 2006).
Few research works proposed alternative column bases with the goal of overcoming the shortcomings of conventional column bases. Mackinven *et al.* (2007) proposed a steel column base with unbounded

[1]Lecturer, Dept. Civil, Environment & Geomatic Eng., Univ. College of London, UK, F.Freddi@ucl.ac.uk
[2]Marie-Curie Research Fellow, School of Eng., University of Warwick, UK, dchristoforos@hotmail.com
[3]Professor, Faculty of Eng. and the Environment, University of Southampton, UK, T.Karavasilis@soton.ac.uk

steel bars that act as re-centering devices while the column experiences rocking under lateral loads. This column base lacks energy dissipation and develops significant stress concentration during rocking. MacRae *et al.* (2009) proposed a steel column base where a pin is used to resist axial and shear forces. Flexural resistance and energy dissipation is provided by friction due to relative movement of the column flanges with respect to foundation flange plates with slotted holes. This column base has minimal-damage behaviour in the strong column axis direction. Yamanishi *et al.* (2012) developed a steel column base that involves exposed yield bolts anchored on a strong plate welded on the column and connected to the foundation anchor bolts through couplers. The yield bolts are the only components that experience damage and can be easily replaced. Chi and Liu (2012) developed a damage-free steel column base that involves post-tensioned (PT) bars anchored at the mid-story height and at the bottom of a grade steel beam. Energy dissipation is provided by buckling-restrained steel plates, while shear resistance by bolted keeper plates. Chou and Chen (2011) developed a similar self-centering column base but with PT bars anchored at the top and at the base of the first story columns. Borzouie *et al.* (2016) presented experimental results on a column base using an asymmetric friction connection. The system experiences rocking and dissipate energy with friction/sliding surfaces parallel to the column strong axis. Superior behaviour was achieved under loading in the column strong axis direction, while damage and stiffness degradation were observed under loading in the column weak axis direction.

Freddi *et al.* (2017) recently proposed and numerically investigated a rocking damage-free steel column base, which uses PT high-strength steel bars to control rocking behaviour and friction devices (FDs) to dissipate seismic energy. The column base monotonic and cyclic moment–rotation curves are described with the aid of simple analytical equations that consider different limit states. In addition, a design procedure based on nondimensional parameters and a simple graphical tool was presented. Analytical moment–rotation equations and the design procedure were validated with 3D nonlinear finite element (FE) simulations in ABAQUS. In addition, a simplified 2D model of the rocking column base was developed in OpenSees to conduct nonlinear dynamic analyses on a steel self-centering moment resisting frame (SC-MRF) using either conventional or the proposed column base. The comparison showed that the rocking column base fully protects the first story columns from yielding and eliminates the first story residual drift. The present paper experimentally evaluates a 3/5-scaled specimen of the rocking damage-free steel column base under monotonic and cyclic loading histories. The experimental program includes also tests for the characterization of the FDs. The experimental results are presented and discussed in detail in the following Sections.

2. ROCKING DAMAGE-FREE STEEL COLUMN BASE

Figure 1 shows the column base proposed by Freddi *et al.* (2017). A thick steel plate with rounded edges is welded on the bottom of a circular hollow section. The rounded edges avoid stress concentration and damage during rocking. Four PT high strength steel bars are symmetrically placed around the center of the column base to control the rocking behaviour. The PT bars are anchored to the bottom of the foundation and to an anchor plate welded on the top of the hollow section (Figure 1(a)). FDs are placed to the four sides of the column base to provide energy dissipation during rocking. The FDs consist of two external steel plates bolted to the base plate; an internal steel plate welded to the circular hollow section; and two plates of brass material in the interface. Rocking of the column base results in sliding of the internal plate with respect to the brass and external plates, and thus, in energy dissipation due to friction. The internal plate is drilled with inclined slotted holes to enable sliding, while the external plates and the brass plates are drilled with aligned rounded holes to accommodate pre-tensioned bolts that are used to tune the friction force.

Figure 2(a) shows the dimensions of the column base that control the moment-rotation behaviour, *i.e.* b is the dimension of the contact surface; b_{PT} is the distance among the PT bars; b_{FD} is the distance among the centers of the FDs and h_{FD} is the distance of the centers of the FDs from the base plate. Figure 2(b) shows the column base at the onset of rocking with respect to its right edge. $F_{PT,u}$ and $F_{PT,d}$ are the forces in the PT bars, while $F_{FD,u}$, $F_{FD,d}$ and $F_{FD,c}$ are the forces in the FDs. The subscripts u and d denote whether the point of application of these forces will move upward or downward during rocking. The subscript c denotes the force in central FDs. The lever arms of the forces with respect to

the center of rotation $z_{PT,u}$, $z_{PT,d}$, $z_{FD,u}$, $z_{FD,c}$, $z_{FD,d}$ are derived from the geometry (Freddi *et al.* 2017).

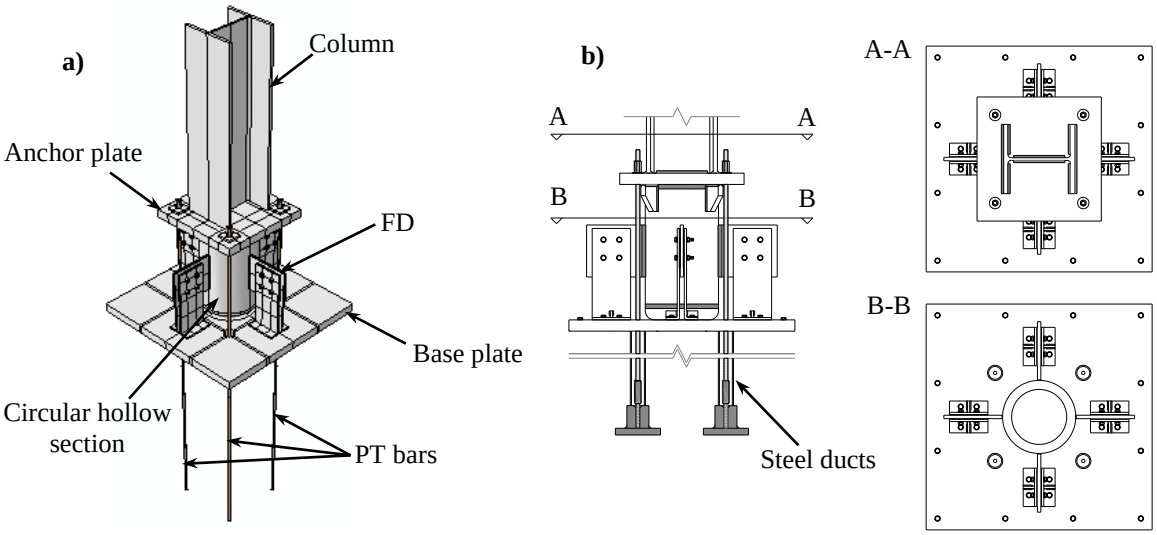

Figure 1. Proposed column base (a) 3D view and (b) lateral view and sections

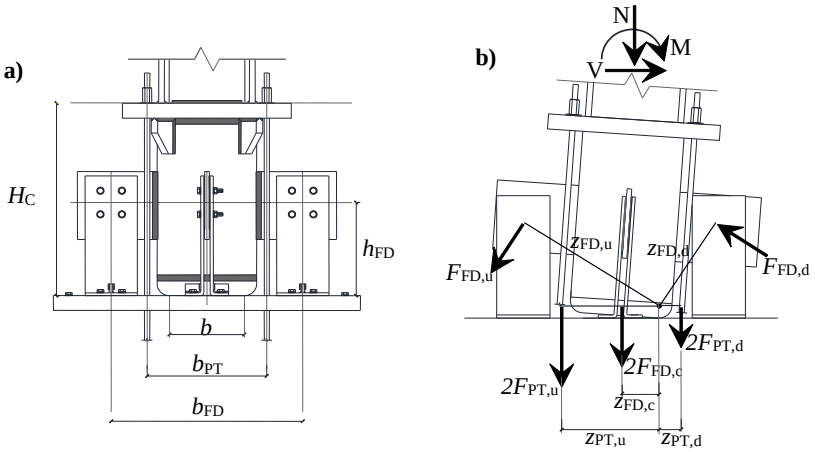

Figure 2. Column base (a) fundamental dimensions, (b) forces and lever arms of the friction devices (FDs) and post-tensioned (PT) bars during rocking for loading from left to right

The moment contributions of the axial force, M_N, of the PT bars, M_{PT} and of the FDs, M_{FD} are reported in Figure 3(a) and are given by

$$M_{\mathrm{N}} = Nb/2 \tag{1}$$

$$M_{\mathrm{PT}}(\theta) = 2\left[T_{\mathrm{PT}}\left(z_{\mathrm{PT,u}} - z_{\mathrm{PT,d}}\right) + K_{\mathrm{PT}}\left(z_{\mathrm{PT,u}}^2 + z_{\mathrm{PT,d}}^2\right)\theta\right] \qquad for\ \theta \le \theta_{\mathrm{T}} \tag{2}$$

$$M_{\mathrm{FD}} = 2 \cdot F_{\mathrm{FD}}\left(z_{\mathrm{FD,u}} + 2 \cdot z_{\mathrm{FD,c}} + z_{\mathrm{FD,d}}\right) \tag{3}$$

where T_{PT} is the initial post-tensioning force of each PT bar; $K_{PT} = E_{PT}A_{PT}/L_{PT}$ is the stiffness of each PT bar; E_{PT}, A_{PT} and L_{PT} are respectively the Young's modulus, the cross-sectional area and the length of each PT bar and $F_{\mathrm{FD,i}}$ is the friction force for each friction surface of the FDs.
The decompression moment, M_{E}, and the moment at the onset of rocking, M_{D}, are given by

$$M_{\mathrm{E}} = M_{\mathrm{N}} + M_{\mathrm{PT,0}} \qquad M_{\mathrm{D}} = M_{\mathrm{E}} + M_{\mathrm{FD}} \tag{4}$$

where $M_{\mathrm{PT,0}}$ is the moment provided by the PT bars at zero rotation, *i.e.* θ = 0.0 in Equation 2. The

rotational stiffness contribution of the PT bars, S_{PT}, and the moments corresponding to points 1 to 4 of the cyclic M-θ behaviour reported in Figure 3(b) are given by

$$S_{PT} = 2K_{PT}\left(z_{PT,u}^2 + z_{PT,d}^2\right) \quad (5)$$

$$M_1 = M_D = M_N + M_{PT,0} + M_{FD} \quad (6a)$$

$$M_2 = M_D + S_{PT}\theta_2 \quad (6b)$$

$$M_3 = M_D + S_{PT}\theta_2 - 2M_{FD} \quad (6c)$$

$$M_4 = M_D - 2M_{FD} \quad (6d)$$

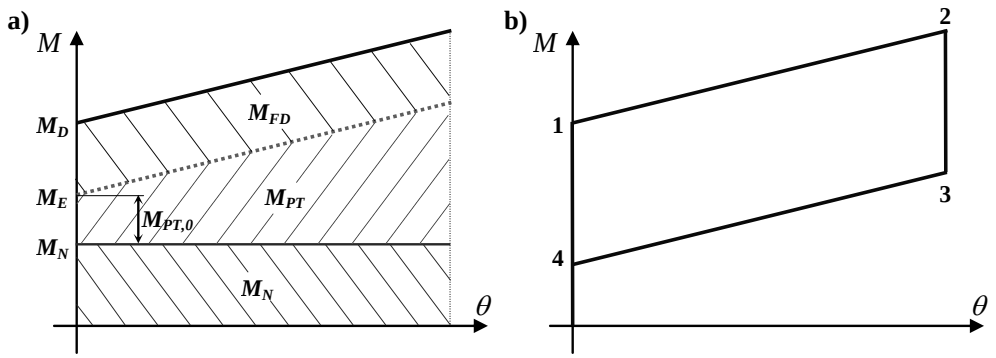

Figure 3. Moment-rotation behaviour of the column base. (a) Moment contribution of the axial force, M_N; of the PT bars, M_{PT}; and of the FDs, M_{FD}; (b) hysteretic behaviour

3. SPECIMEN DESIGN

A column with cross-section HEB 300 is extracted from a prototype building and used to define the specimen of the experimental study. The minimum and maximum axial forces, N_{Ed}, deriving from the seismic load combination are equal to 510.3 kN and 565.3 kN, respectively. The axial force due to the gravity loads of the seismic load combination, $N_{Ed,G}$, is equal to 537.8 kN.

The experimental test is conducted on a 3/5 scaled model (scaling factor $\lambda = 0.6$) of the full-scale prototype column base. The specimen of the column base used in the experimentation is designed based on the dimensions of the scaled column cross-section, the scaled values of the axial forces N_{Ed} and $N_{Ed,G}$, and the target drift defined for the prototype building. The scaling factor $\lambda = 0.6$ is chosen based on the Lab capabilities. Length units are scaled by λ, while areas and forces are scaled by λ^2.

The column base chosen for the experimental test is a UC 203×203×46, which has similarities with the dimensions of the prototype column base HEB 300 scaled by λ. The scaled axial forces N_{Ed} and $N_{Ed,G}$ are equal to 203.5 kN and 193.6 kN, respectively. The target rotation is assumed equal to $\theta_T = 0.03$ rad. The bending moment resistance $M_{N,Rd}$ evaluated according to the Eurocode 3 is equal to $M_{N,Rd,y}$ = 176.58 kNm and $M_{N,Rd,z}$ = 81.97 kNm in the strong and weak column axis, respectively.

Based on the geometry of the column cross-section, the fundamental dimensions of the column base (*i.e.* b, b_{PT}, b_{FD}, and h_{FD}) are selected with respect to practical and geometric considerations. A circular hollow section with 193.7 mm diameter and 30 mm thickness is adopted. A circular steel plate with the same diameter is welded at the bottom of the hollow section. Standard mechanical processing provides this plate with rounded circular edges having a radius of 30 mm as well as with appropriate space to accommodate the shear key. The contact surface has a dimension b equal to 143 mm. Due to the reduced availability of PT bars of small dimensions, 7 wire strands satisfying the requirements of the BS 5896 (BSI Standards Publication, 2012) have been used in the experiment. The anchor plate of the post-tensioned strands in the top of the hollow steel section is rectangular and has width, length and thickness equal to 330 mm, 415 mm and 50 mm, respectively. The distance among the strands b_{PT} is selected equal to 255 mm. Table 1 provides the material properties assumed for the design (f_y: yield

stress; f_u: ultimate stress; E: Young's modulus) according to test certificates provided by the suppliers.

Table 1. Design properties of the materials

Elements		f_y **[MPa]**	f_u **[MPa]**	E **[GPa]**
Column and plates	S 355 JR	355	510	210
Post-tensioned strands	BS 5896:2012	1885	1995	195
Bolts	Class 10.9	900	1000	210
Brass	C46400 half hard	200	450	100

The design is performed according to the methodology proposed by Freddi *et al.* (2017), which is based on the use of Equations 7 below

$$\kappa = \frac{1}{2A_{PT} f_{y,PT} \left(z_{PT,u} - z_{PT,d}\right)} \left[\frac{M_T - 2\frac{E_{PT} A_{PT}}{L_{PT}} \left(z_{PT,u}^2 + z_{PT,d}^2\right)\theta_T}{1 + \frac{1}{\alpha_{sc}}} - N_{Ed,G} \frac{b}{2} \right] \tag{7a}$$

$$\kappa \le 1 - \frac{E_{PT} \cdot z_{PT,u} \cdot \theta_T}{f_{y,PT} \cdot L_{PT}} = \kappa_{max} \tag{7b}$$

$$\kappa \ge \frac{E_{PT} \cdot z_{PT,d} \cdot \theta_T}{f_{y,PT} \cdot L_{PT}} = \kappa_{min} \tag{7c}$$

where $M_T = M_{N,Rd}/\gamma_T$ is the moment at the target rotation, which through the safety coefficient γ_T, allows to protect the column from yielding, while $\gamma_{sc} = M_E/M_{FD}$ is a design parameter that controls the self-centering capability of the column. A_{PT}, L_{PT} and κ are the design variables of the problem *i.e.* the area of the post-tensioned strands, the length of the post-tensioned strands, and ($\kappa = \sigma_{PT}/f_{y,PT}$) the stress ratio in the strands, where σ_{PT} and $f_{y,PT}$ are the stress and the yield stress of the strands that allow to define the value of the initial post-tensioning force.

Figure 4(a) shows the variation of κ with respect to L_{PT} for 7 wire strands of 9.3 mm, with an equivalent area of A_{PT} = 52 mm^2. The coefficients γ_T and γ_{sc} have been assumed respectively equal to 1.165 and 1.10. The design procedure provides L_{PT} equal to 805 mm and κ equal to 0.2175 (T_{PT} = 21.3 kN). The rotations $\theta_{PT,u,y}$ and $\theta_{PT,d,f}$ are equal to 0.0306 rad and 0.0302 rad, respectively. $\theta_{PT,u,y}$ is the rotation at which the PT bars (in position *u*) yield; and $\theta_{PT,d,f}$ is the rotation at which the force of the PT bars (in position *d*) becomes zero, *i.e.* when loss of post-tensioning occurs.

Figure 4(b) shows the moment-rotation behaviour for the column base. The decompression moment, M_E, the moment at the onset of rocking, M_D, and the moment provided by the FDs, M_{FD}, are equal to 19.94 kNm, 38.07 kNm and 18.13 kNm, respectively.

M_{FD} is derived by M_E and α_{sc}, then, the FDs can be designed by selecting appropriate values of the parameters of Equation 3. FDs are introduced on the four sides of the column base and the relevant dimensions are b_{FD} = 465 mm and h_{FD} = 250 mm. The required friction force in each of the four FDs is F_{FD} = 10.87 kN. The thickness of the internal and external plates of the FDs are 10 mm and 8 mm, respectively. Two 3 mm thick brass plates are used as friction interfaces and two M12 class 10.9 bolts are used to apply the pre-loading force by tightening. The friction coefficient at the brass-steel interface is evaluated by preliminary tests described in the next section. The pre-loading force is defined based on the friction coefficient in order to achieve the required friction force. The dimensions of the slotted holes are designed to allow a large rotation (*i.e.* close to 0.06 rad) without bearing of the bolts on the plates. Figure 5 summarizes the geometry of the column base.

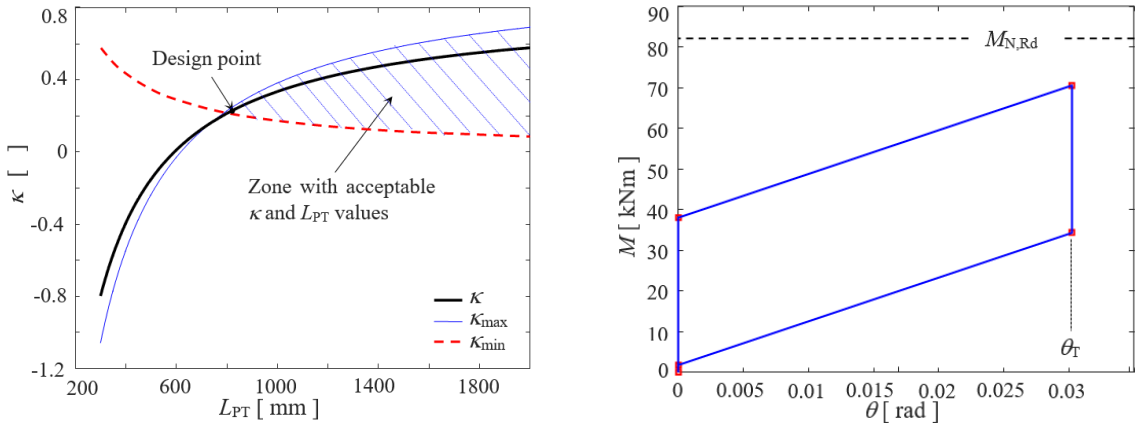

Figure 4. (a) Variation of κ with respect to L_{PT} for A_{PT} = 52 mm^2 and (b) M-θ behaviour of the column base

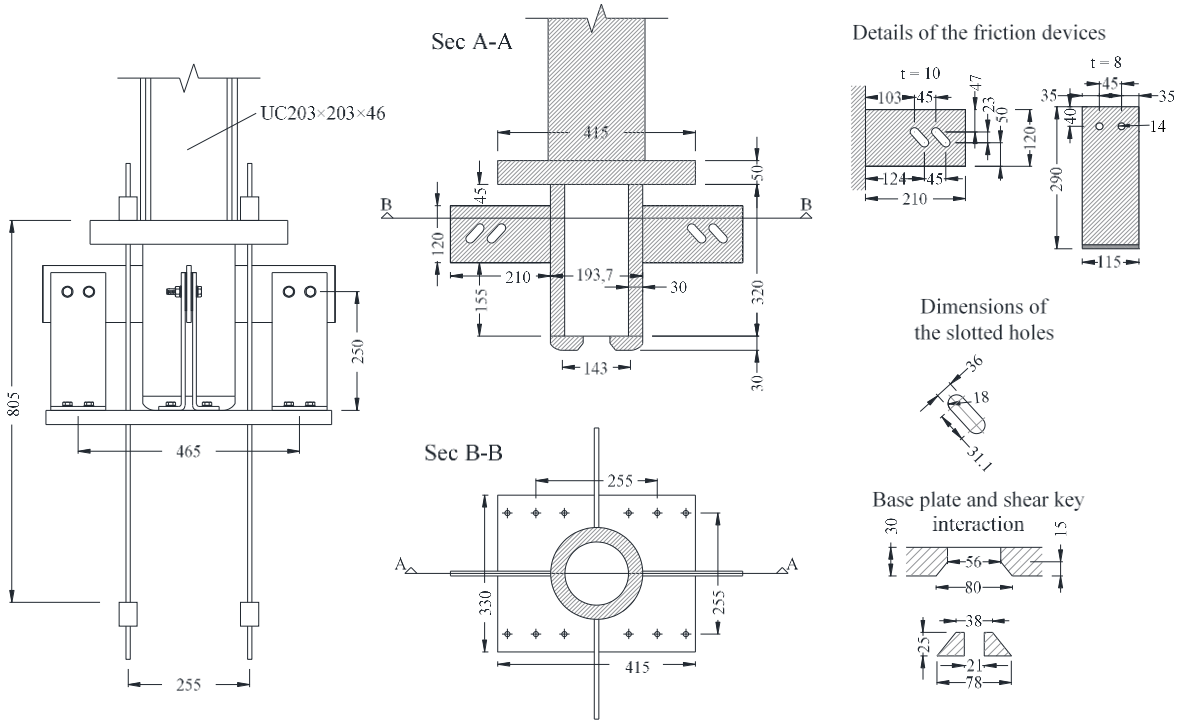

Figure 5. Geometry of the specimen (dimension in mm)

4. INTRUMENTATION FOR THE TESTS

The instrumentation required to perform the tests include: *i)* Main Actuator to apply the horizontal load on the column plus 6 hydraulic jacks for the post-tensioning of strands and PT bars (Table 2); *iii)* 12 load cells in order to monitor the forces in the strands, PT bars and bolts of the FDs (Table 3); *iv)* 4 Linear variable differential transformer (LVDT) to measure the displacements and *v)* 4 strain gages positioned at the base of circular hollow section in order to evaluate possible yielding.

Table 2. Hydraulic systems

Actuator	Acronym	Use	Max force [kN]	Stroke [mm]
***		Application of the horizontal force	293	±150
Hi-Force HHS102	HJA	Post-tensioning of strands	110	+50
Yale YCS 57-70	HJB	Post-tensioning of PT bars	567	+70

Table 3. Load Cells

Load Cells	Acronym	Measuring	Max force [kN]
Novatech F207	LCA	Axial force in the bolts of the friction devices	80
Novatech F313	LCB	Axial force in the 7 wire strands (9.3 mm)	200
Novatech F203	LCC	Axial force in the PT bars (15 mm)	600

5. FRICTION DEVICE CHARACTERIZATION

The friction force, $F_{FD,i}$, for each friction surface is given by

$$F_{FD,i} = \mu_{FD} \cdot n_b \cdot N_b \quad with \ i = u,c,d \tag{8}$$

where μ_{FD} is the friction coefficient of the surfaces in contact; n_b is the number of bolts and N_b is the bolt pre-loading force. The bolts pre-loading force can be determined from the tightening torque by means of the following equation according to Latour *et al.* (2015).

$$N_b = T_b / \alpha d \tag{9}$$

where T_b is the value of the tightening torque, d is the bolt diameter and α is conventionally assumed equal to 0.2. The application of a tightening torque according to Equation 9 allows to obtain the desired bolt pre-loading force, N_b, with an accuracy of +20%. Such scatter is due, on one hand, to the difficulties arising in the control of the tightening torque, and on the other hand, to the variable stiffness of the clamped surfaces.
The objectives of the preliminary tests for the characterization of the FDs are: *i)* definition of the relationship between tightening torque, T_b, and the bolt pre-loading force, N_b, for the specific case; *ii)* definition of the friction coefficient, μ_{FD}, for the specific materials interface.

5.1 Relationship between torque and the bolt pre-loading force

In order to define of the relationship between T_b and N_b for the specific case, 30 bolts with 9 different torque values from 20 up to 100 Nm have been tested. The tightening torques have been applied by means of a calibrated torque wrench (Norbar PRO 100 1/2"), while the pre-loading force in the bolts is measured through load cells (LCA in Table 3). Figure 6(a) shows the test setup used for measuring the pre-loading forces imposed by the torque force. The coefficient α, of Equation 9, for the specific case is evaluated based on the linear interpolation of a total of 270 samples and takes a value of $\alpha = 0.1743$. The results of the tests are reported in Figure 6(b) together with the interpolation line and the relationship based on the recommended value for $\alpha = 2$. This part of the study allows to specialize the correlation for the bolts used in the experimentation in order to increase the confidence in the friction force obtained by the FDs. The error in the evaluation of the pre-loading force is about of 20%; thus, confirming previous findings reported in literature.

5.2 Tests for the friction coefficient of the materials interface

In order to define the value of the friction coefficient, μ_{FD}, for the investigated materials and to assess its stability, cyclic tests have been performed on the FD. In this test setup, to allow the relative displacements between the plates in the friction surface and to accommodate the travel path of the bolts, the inner plate has been realized with slotted holes with dimensions of 44 by 15 mm. The other inner brass friction plates and the two outer steel plates have been realized with circular holes. The clamping force has been applied by means of two M12 bolts 10.9 class. The dimensions of the surface in contact is the same with those in the FDs of the column base specimen. Quasi-static tests using four values of the pre-loading force in each bolt have been performed spanning from 10 to 25 kN; thus,

obtaining different values of the clamping force acting on the sliding surface. The brass material used in the tests is 'C46400 half hard' type, while the material used for the steel components is the 'S355 JR'.

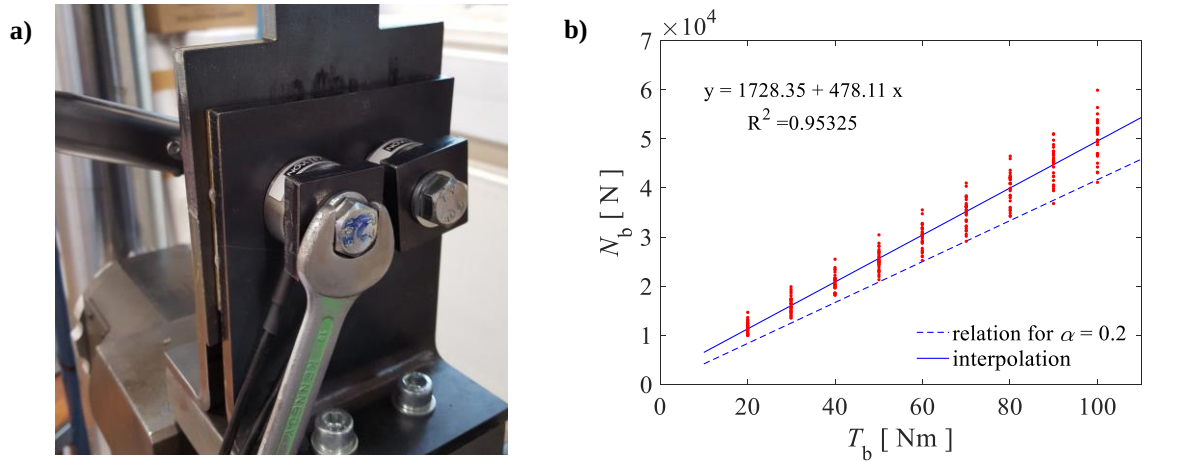

Figure 6. Test for the characterization of the relationship between the tightening torque T_b and the bolt pre-loading force N_b. (a) Test setup; (b) test results and interpolation curve

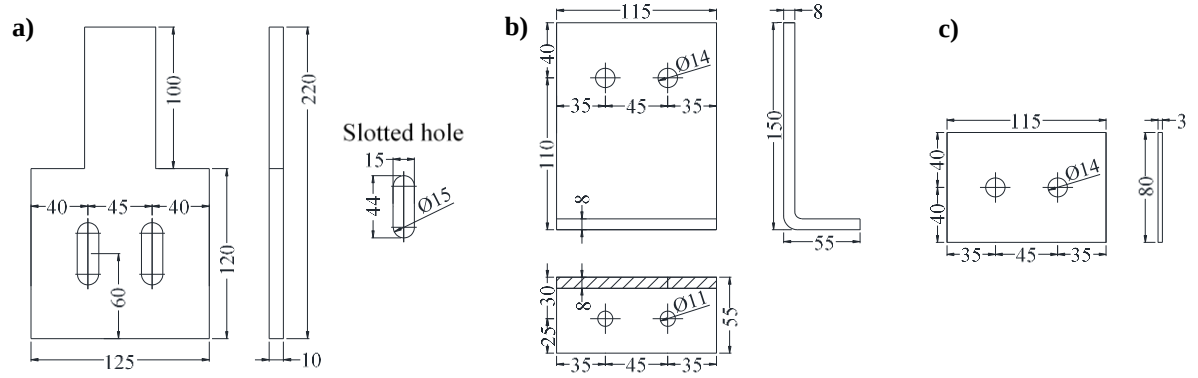

Figure 7. Components for the tests of the friction devices (FDs). (a) Internal plate with slotted holes; (b) external plate and (c) brass plate. (dimensions in mm)

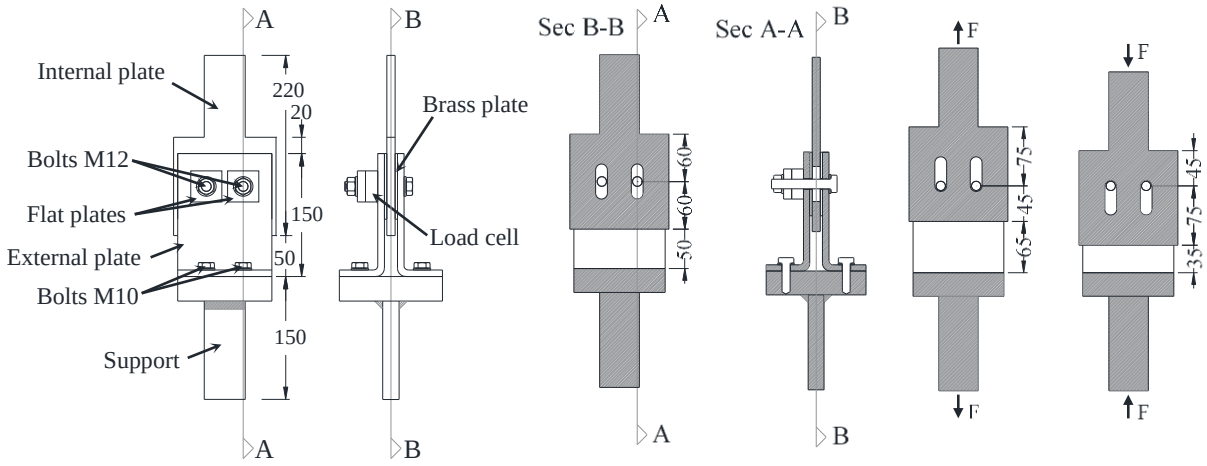

Figure 8. Tests for the definition of the friction coefficient (dimensions in mm)

The tests have been carried out by means of the universal testing machine DARTEC 9500. The testing

equipment is constituted by a hydraulic piston with a 250 kN load cell. The upper and lower inner plates are clamped between the hydraulic grips. The tests have been carried out under 20 loading cycles with a linear variation of the applied displacement, a constant amplitude of ±10 mm, and a frequency equal to 0.25 Hz. The pre-loading force has been increased at the end of each loading sequence starting from 10 kN up to 25 kN and the tests have been performed at intervals of 30 minutes in order to avoid a significant increase of the temperature that could affect the friction behaviour of the interface. The axial force in the bolts, N_b, is monitored with load cells during the tests. The friction coefficient has been determined as

$$\mu_{FD} = F_{FD} / m \cdot n \cdot N_b \tag{10}$$

where m = 2 is the number of surfaces in contact and n = 2 is the number of bolts. Figure 9 reports the results of the test with the pre-loading force in the bolts equal to 16.5 kN. The average pre-loading force acting on the friction interface and given by the sum of the average force in the two bolts along the duration of the test is equal to 33.472 kN. Figure 9(a) shows the force-displacement history, while Figure 9(b) shows the friction coefficient obtained according to Equation 10. Consistent results have been obtained also for the other pre-loading force values.

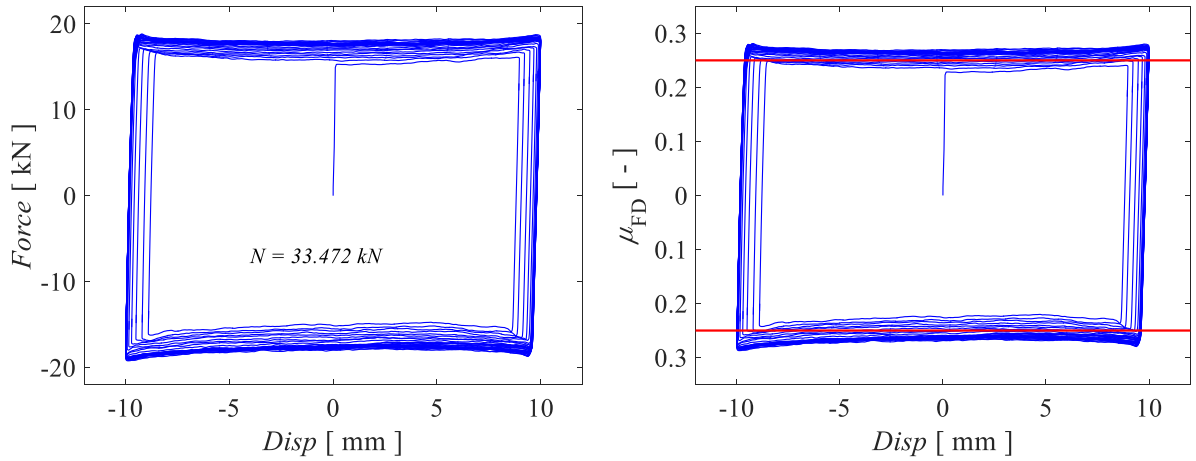

Figure 9. Tests on the friction device (FD) with initial preloading force in each bolt of 16.5kN. (a) displacement – force hysteretic curve; (b) normalized force for the definition of the friction coefficient μ_{FD}.

6. TESTS ON THE ROCKING DAMAGE-FREE COLUMN BASE

Experiments on the proposed rocking damage-free steel column base with FDs were conducted in the test setup shown in Figure 10. Two external PT bars with diameter of 15 mm (A_{PT} = 177 mm^2) and yield and ultimate strength equal to f_y = 900 MPa and f_u = 1100 MPa, are introduced to simulate the axial force due to the gravitational load. The PT bars are connected to the upper beam, which transfers the force to the column, and to two anchor supports connected to the strong floor. The hollow hydraulic jacks type B (HJB in Figure 10) are used in order to apply the post-tensioning force and the load cells type C (LCC 1 & 2 in Figure 10) are used to measure and to calibrate the initial force and to control its variation during the tests. The column is placed on a steel basement provided with anchor plates for the strands. The strands are post-tensioned through hollow hydraulic jacks type A (HJA in Figure 10) and four load cells type B (LCB in Figure 10) are interposed between the anchor grips and the anchor plates in order to calibrate the initial post-tensioning force and to measure the force variation along the tests. The pre-loading force in the FDs is applied through a calibrated torque wrench based on Equation 8. Four load cells type A (LCA in Figure 10) are used to measure the variation of the axial force in the bolts during the tests. The shear key is fixed to the steel basement through a bolt M20.

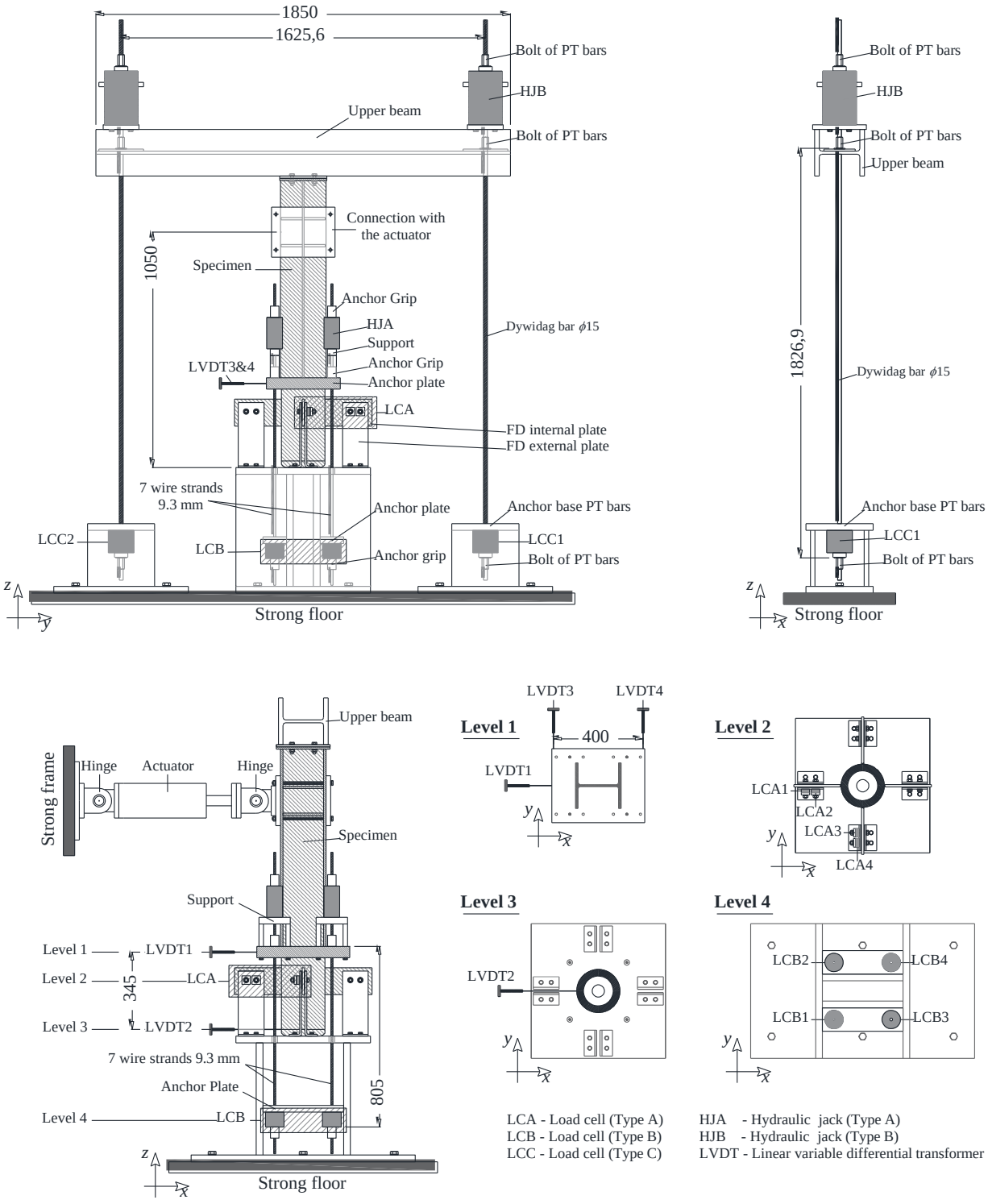

Figure 10. Tests Setup and instrumentation (dimensions in mm)

The specimen is connected to the horizontal actuator, which is connected to a strong steel frame. The actuator is connected at both the ends by hinges in order to avoid any transfer of moment to the column. LVDTs are placed on the base of the column in order to measure horizontal translations and rotations in the longitudinal direction, as well as, horizontal translations in the transverse direction and torsions. Moreover, in order to evaluate the stresses and deformation of the circular hollow cylinder of the column base, four strain gages are introduced in the position close to the pivot points of the rocking at each side. While rocking, the uplift of the column base will produce an increase of the force

in the external PT bars. Records of the forces history is provided by the load cells (LCC 1 & 2 in Figure 10). The upper beam is designed in order to behave elastically during the test.
Quasi static experimental tests have been performed on the column base with and without strands and FDs in order to decouple the moment contributions from each component. Preliminary tests have been performed with amplitudes ranges within the elastic behaviour of the strands ('small' amplitudes). Figure 11(a) shows the force-displacement history from the test including all the components for 'small' amplitudes, while Figure 11(b) shows the variation of force in the strands. A final test with cyclic displacements of increasing amplitude have been conducted showing the damage-free behaviour of the column base up to the design rotation. For amplitudes higher than the design rotation, yielding of the strands occur, while, for very large rotation the failure is observed in the FDs due to bolts bearing (such failure could be avoided with longer slotted holes in the internal steel plate of the FDs).

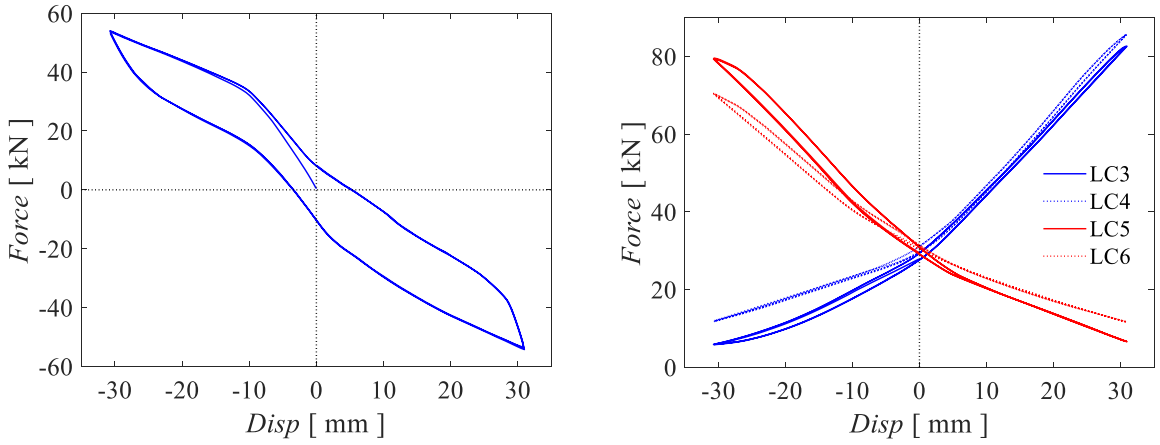

Figure 11. Cyclic test of the column base with friction device (FD) (a) displacement – force hysteretic curve; (b) tension force in the strands.

7. CONCLUSIONS

This paper describes experiemental tests on a damage-free rocking steel column base with friction devices, previously proposed and numerically investigated by the authors. The column base uses post-tensioned (PT) high strength steel bars to control rocking behaviour and friction devices (FDs) to dissipate seismic energy. A column base extracted from a prototype steel building was designed using a step-by-step design procedure aiming to achieve damage-free and self-centering behaviour for a predefined target rotation. Components tests for the characterization of the FDs have been conducted to assess the relationship between the torque applied to high-strength bolts and the resistance (force corresponding to initiation of sliding) of the FDs. Monotonic and cyclic tests were conducted on a 0.6-scale column base. The experimental show good agreement with the expected (predicted with the aid of analytical equations) behaviour and confirm that the column base has damage-free and self-centering behaviour up to the design rotation.

8. ACKNOWLEDGMENTS

This research is supported by Marie Sklodowska-Curie Action Fellowships within the H2020 European Programme. Any opinions, findings, and conclusions or recommendations expressed in this paper are those of the authors and do not necessarily reflect the views of the European Commission. The Authors also gratefully acknowledge the support of Prof. J. Toby Mottram and the work of the technicians of the Structural Testing Laboratory of the University of Warwick: Taylor Arnett and Neil Gillespie.

9. REFERENCES

Christopoulos C, Filiatrault A (2006). Principles of passive supplemental damping and seismic isolation. IUSS Press, Pavia, Italy.

Chancellor NB, Eatherton MR, Roke DA, Akbas T (2014). Self-centering seismic lateral force resisting systems: High-performance structures for the city of tomorrow. *Buildings*, 4: 520-548.

Eurocode 3 (2005). Design of steel structures – Part 1.8: Design of Joints. *European Committee for Standardization*, Brussels, Belgium.

Eurocode 8 (2005). Design of structures for earthquake resistance. Part 1: General rules, seismic action and rules for buildings. *European Committee for Standardization*, Brussels, Belgium.

Latour M, Rizzano G (2013a). Full strength design of column base connections accounting for random material variability. *Engineering Structures*, 48: 458–471.

Latour M, Rizzano G (2013b). A theoretical model for predicting the rotational capacity of steel base joints. *Engineering Structures*, 91: 89–99.

Kanvinde AM, Grilli DA, Zareian F (2012). Rotational stiffness of exposed column base connections: experiments and analytical models. *J. Struct. Eng.*, 138(5), 549–560.

Grauvilardell J.E., Lee D., Hajjar J.F., Dexter R.J. "Synthesis of design, testing and analysis research on steel column base plate connections in high-seismic zones". Report ST-04-02, Dept. of Civil Engineering, Univ. of Minnesota, USA, 2006.

Mackinven H, MacRae GA, Pampanin S, Clifton GC, Butterworth J (2007). Generation four steel moment frame joints. *Proceedings of the 8th Pacific Conference on Earthquake Engineering*, Singapore.

MacRae GA, Urmson CR, Walpole WR, Moss P, Hyde K, Clifton C (2009). Axial shortening of steel columns in buildings subjected to earthquakes. *Bulletin of the New Zealand Society for Earthquake Engineering*, 42(4): 275–287.

Yamanishi T, Kasai K, Takamatsu T, Tamai H (2012). Innovative column-base details capable of tuning rigidity and strength for low to medium-rise steel structures. *Proceedings of the 15th World Conference on Earthquake Engineering*, Lisbon, Portugal.

Chi H, Liu J (2012). Seismic behaviour of post-tensioned column base for steel self-centering moment resisting frame. *Journal of Constructional Steel Research*, 78: 117–130.

Chou C-C, Chen JH (2011). Analytical model validation and influence of column bases for seismic responses of steel post-tensioned self-centering MRF systems. *Engineering Structures*, 33(9): 2628–2643.

Borzouie J, MacRae GA, Chase JG, Rodgers GW, Clifton GC (2016). Experimental studies on cyclic performance of column base strong axis – aligned asymmetric friction connections. *Journal of Structural Engineering* (ASCE), 142(1): 04015078.

Freddi F, Dimopoulos CA, Karavasilis TL (2017). Rocking damage-free steel column base with friction devices: design procedure and numerical evaluation. *Earthquake Engineering & Structural Dynamics*, 46(14): 2281–2300. DOI: 10.1002/eqe.2904.

Latour M, Piluso V, Rizzano G (2015). Free from damage beam-to-column joints: Testing and design of DST connections with friction pads. *Engineering Structures*, 85, 219–233.